AGU100 ADVANCING EARTH AND SPACE SCIENCE

Geophysical Research Letters

RESEARCH LETTER
10.1029/2019GL086022

A Full-Spectrum Bedrock Thermal Expansion Model and Its Impact on the Global Positioning System Height Time Series

Jintao Lei[1], Wu Chen[1], Zhao Li[1], Fei Li[2], and Shengkai Zhang[2]

[1]Department of Land Surveying and Geo-Informatics, Hong Kong Polytechnic University, Hong Kong, China, [2]Chinese Antarctic Center of Surveying and Mapping, Wuhan University, Wuhan, China

Key Points:
- We use FEM to calculate the full-spectrum bedrock thermal expansion displacement, including seasonal terms and nonseasonal variations
- Nonseasonal deformation can reach 3 mm in some regions, and its mean power accounts for 20% of the entire thermal expansion
- Nonseasonal variations can be detected by geodetic observations and thus cannot be ignored

Supporting Information:
- Supporting Information Figure S1
- Supporting Information Data S1

Correspondence to:
W. Chen,
wu.chen@polyu.edu.hk

Citation:
Lei, J., Chen, W., Li, Z., Li, F., & Zhang, S. (2020). A full-spectrum bedrock thermal expansion model and its impact on the Global Positioning System height time series. *Geophysical Research Letters*, *47*, e2019GL086022. https://doi.org/10.1029/2019GL086022

Received 28 OCT 2019
Accepted 21 DEC 2019
Accepted article online 3 JAN 2020

Abstract Bedrock thermal expansion includes prominent seasonal (annual and semiannual) terms and intricate nonseasonal variations (high-frequency change and transient signals). However, the nonseasonal variations are usually ignored in geodetic studies due to defects in analytical solutions. In this study, we calculate the full-spectrum bedrock thermal expansion displacement using the skin temperature from the ERA5 reanalysis data set. The results show that the nonseasonal variations of bedrock thermal expansion, with a range (maximum minus minimum) reaching 3 mm in some regions, can be observed by geodetic instruments and thus cannot be ignored. Moreover, the mean power of the nonseasonal variations accounts for 20% of the entire thermal expansion. Without considering the influence of the nonseasonal variations, this "noise" would remain in the original observations and contaminate related geophysical inversions.

Plain Language Summary Like any natural material, bedrock exhibits thermal expansion, resulting in volume variations in response to surface temperature changes. Previous studies on the analytical calculations of bedrock thermal expansion indicated that harmonic expansion of the surface temperature in the time or space domain was required. This type of harmonic method could consider only seasonal (annual and semiannual) terms and would inevitably ignore nonseasonal variations such as high-frequency change and transient signals. To avoid this disadvantage, we use the finite element method to numerically calculate the full-spectrum bedrock thermal expansion and then study its seasonal and nonseasonal impacts on the Global Positioning System height time series. Our results demonstrate that the range (maximum minus minimum) of nonseasonal variations can reach 3 mm and can be observed by Global Positioning System height time series. Considering the nonseasonal variations of bedrock thermal expansion allows us to study other geophysical phenomena with higher precision and accuracy.

1. Introduction

The Earth's lithosphere is always in motion due to factors including mass redistribution (Tregoning & van Dam, 2005; Fu et al., 2012;), plate tectonics (Koulali et al., 2011; Serpelloni et al., 2013), and earthquakes (Feng et al., 2010; Galetzka et al., 2015). Global Positioning System (GPS) technology has been widely used to investigate mass and non-mass signals (Fu et al., 2015; Ji & Herring, 2011). Previous studies have shown good consistency between GPS and GRACE (Gravity Recovery and Climate Experiment) or load models in regions with large mass signals (Chanard et al., 2014; Hao et al., 2016; Pan et al., 2018; Yan et al., 2016). However, the annual signals in GPS only decrease to a certain extent when applying corrections from GRACE or load models at the global scale (Dong et al., 2002; Zou et al., 2014). The apparent inconsistency in the long-term trends and interannual terms between GPS and GRACE/load models also limit their combined use in studies of nonseasonal variations (Han, 2017; Santamaría-Gómez & Mémin, 2015). In addition to the known errors and limitations of GPS/GRACE/load models, other non-mass signals, such as bedrock thermal expansion, can cause inconsistencies as well (Dong et al., 2002; Fang et al., 2013; Yan et al., 2009).

A temperature change will cause thermal expansion of the monument and bedrock under a GPS antenna (Berger, 1975). Based on a half-space model, Dong et al. (2002) calculated the bedrock thermal expansion displacement (TED) with a vertical annual amplitude of 0.56 mm. Yan et al. (2009) extended the half-space model to other frequencies and found that the vertical annual amplitude of TED could reach 1.3 mm in some regions. By using the uniform elastic sphere model developed by Fang et al. (2013), Xu et al. (2017) investigated the influence of bedrock thermal expansion on GPS time series and found that the annual amplitude

reaches approximately 3 mm for radial displacement and approximately 1.5 mm for transverse components. All these studies are based on an analytical calculation of TED, indicating that harmonic expansion of the surface temperature in the time or space domain is required. In this way, only seasonal (usually annual and semiannual) terms are considered, whereas nonseasonal variations, such as high-frequency change and transient signals, are inevitably ignored.

With the improvement of computing power, an increasing number of geoscientists have adopted numerical methods to solve partial differential equations (PDEs) (Liu et al., 2018; Quintal et al., 2011). Among them, the finite element method (FEM) can overcome problems related to the smoothness of the input data in the analytic method and have the ability to address complex geometries and various material behaviors (Trasatti et al., 2011; Simpson, 2017). Therefore, we use FEM to calculate the full-spectrum TED and then analyze the impacts of its seasonal terms and nonseasonal variations on the GPS height time series. The paper is organized as follows: Section 2 briefly introduces the numerical solution of TED. The annual term and nonseasonal variations of TED, together with their impacts on selected global GPS height time series, are analyzed in section 3. Conclusions are presented in section 4.

2. Numerical Solution of Bedrock Thermal Expansion

In this paper, only the vertical TED is considered. The one-dimensional PDE of heat conduction is represented by (Berger, 1975; Dong et al., 2002)

$$\frac{\partial T(x,t)}{\partial t} = \kappa \frac{\partial^2 T(x,t)}{\partial x^2} + H \quad (x \in [-l;0]), \tag{1}$$

where $T(x,t)$ is the temperature; $\kappa = 1\ \mathrm{mm}^2/\mathrm{s}$ (Bording et al., 2016; Dong et al., 2002) represents thermal diffusivity; H denotes the internal heat source of the material and the latent heat flux caused by, for example, surface evaporation and condensation (zero in our case); and l indicates the length (depth) of the model. At the Earth's surface, $x = 0$. Two boundary conditions and one initial condition are required to solve this parabolic equation with a second-order spatial derivative and a first-order time derivative:

$$\begin{aligned} T(x=0,t) &= T_{\mathrm{surface}}, \\ T(x=-l,t) &= T_{\mathrm{mean}}, \end{aligned} \tag{2}$$

$$T(x, t=0) = T_{\mathrm{mean}}. \tag{3}$$

The boundary conditions (equation (2)) indicate that the nodal temperature of the model on the Earth's surface is always the same as the instantaneous surface temperature T_{surface} (external force), and the temperature at the deepest part of the model is fixed to the mean surface temperature of the region for a period of time (e.g., 30 years). The initial condition of the model (equation (3)) is set as the nodal temperatures equal to the mean surface temperature when $t = 0$. This initial condition is not practical; therefore, FEM requires a certain initial time so that the nodal temperatures are close to the real temperature.

The procedure of obtaining a numerical solution consists of two steps. The first step is to discretize the continuous PDE with boundary and initial conditions into a series of algebraic equations. The second step is to obtain the temperature of each node by solving the above discrete algebraic equations (Mercer et al., 1975; Simpson, 2017). In our study, the Galerkin FEM was used to numerically solve the nodal temperatures (see supporting information for details). After obtaining the temperature distribution, the TED $h(t)$ can be calculated as follows (Rychlewski, 1984):

$$h(t) = \frac{1+\upsilon}{1-\upsilon} \sum_{i=2}^{n+1} \alpha \cdot x \cdot (T_i - T_{\mathrm{ref}}), \tag{4}$$

where $\frac{1+\upsilon}{1-\upsilon}$ is the gain factor that considers the thermal stress, $\upsilon = 0.25$ represents the Poisson's ratio, $\alpha = 1.5 \times 10^{-5}\ ^{\circ}\mathrm{C}^{-1}$ indicates the coefficient of thermal expansion (Dong et al., 2002; Turcotte & Schubert, 2014; Xu et al., 2017), x is the length (depth) of each element after discretization, T_i denotes the nodal temperature, and T_{ref} is the reference temperature.

The quality of the numerical solution is influenced by various errors and stability. All numerical methods introduce discretization errors and computational errors, among which discretization errors can be reduced by improving the finite element number (spatial resolution), while round-off errors can be controlled by selecting efficient solvers. Stability describes the errors of numerical solution decay with time. However, even a stable solution can still be inaccurate (e.g., due to the existence of bias). Thus, it is also important to assess the accuracy of a numerical solution by directly comparing it with an analytical or approximate solution (Simpson, 2017). Here we use the approximate solution of the harmonic method given by Yan et al. (2009) as a reference:

$$h(t) = \frac{1+\upsilon}{1-\upsilon}\alpha\sum_{i=1}^{n} A_i\sqrt{\frac{\kappa}{\omega_i}}\cos\left(\omega_i t-\varphi_i-\frac{\pi}{4}\right), \tag{5}$$

where υ and α have the same meaning as in equation (4); A_i, ω_i, and φ_i are the amplitude, frequency, and initial phase of the ith harmonic (only annual and semiannual terms in our case) of the surface temperature, respectively. Notably, the summation sign in equation (5) is the summation of n decomposed harmonics of surface temperature, while the summation sign in equation (4) is the summation of TEDs for all elements with different nodal temperatures.

3. Results and Discussion

3.1. Numerical Solution

As mentioned in the previous section, it is not practical to set all the initial nodal temperatures equal to the mean surface temperature. The element number and model depth are also important to the precision of FEM solutions. Through simulation analysis (Figures S1–S3 in the supporting information), the FEM model we use here has an initial time of 5 years, a depth of 100 m and an element number of 10,000. We then use the daily average skin temperature from the ERA5 reanalysis data set to calculate the TED time series for a total of 19 years from 2000 to 2018 (Hersbach, 2018). Skin temperature is defined as the temperature of the surface at radiative equilibrium, and it is derived from the surface energy balance. It forms the interface between soil, snow or ice, and the atmosphere (see ERA5 online documentation for details). The TED time series calculated by the FEM and the harmonic methods for three selected IGS sites (GUAO, LHAZ, and MCM4) are shown in Figure 1, along with their differences (nonseasonal variations) and the local mean annual temperature (root-mean-square with respect to the reference model [number of elements: 10,000; depth: 100 m] as a function of model depth is shown in Figure S4). We can see that FEM can recover the periodic deformation caused by the seasonal terms of temperature and capture the irregularity caused by nonseasonal variations. Although there is a time delay caused by the heat conduction process, the nonseasonal variations of the TED time series shows consistency with the mean annual temperature in the long-term trend. The temperature of the GUAO site is relatively stable, the change in the mean annual temperature for 2000–2018 was less than 4 °C. Correspondingly, the TED time series obtained by the FEM mainly contains seasonal signals, and the nonseasonal variations are less than 1 mm. The LHAZ site is located in Lhasa, China, where the mean annual temperature has been rising in recent years. Consistent with the temperature trend, the TED time series obtained by the FEM contains an uplift signal with a magnitude of approximately 2 mm. This nonseasonal trend, if not considered, can be wrongly attributed to other phenomena, for example, the change of terrestrial water storage, which may lead to incorrect geophysical interpretations. The MCM4 site is located on the Antarctic continent. The FEM-calculated TED time series experiences an upward period from 2004 to 2011 and then becomes stable. Since both bedrock thermal expansion and the melting of ice sheets are both related to temperature change, the seasonal and nonseasonal impacts of the TED must be removed before we use GPS time series to invert the mass loss of ice sheets; otherwise, the result will be contaminated.

3.2. Annual Term of the Bedrock Thermal Expansion Displacement

We use a total of 2,002 GPS height time series provided by the Making Earth Science Data Records for Use in Research Environments project to study the impact of the annual TED on geodetic observations. The GPS height time series has been corrected by conventional geophysical corrections (e.g., solid Earth tide and ocean tide loadings). We also consider the environment loading effects, including the atmosphere, hydrology, and ocean bottom pressure loading, on the GPS height time series. Atmospheric mass loads are

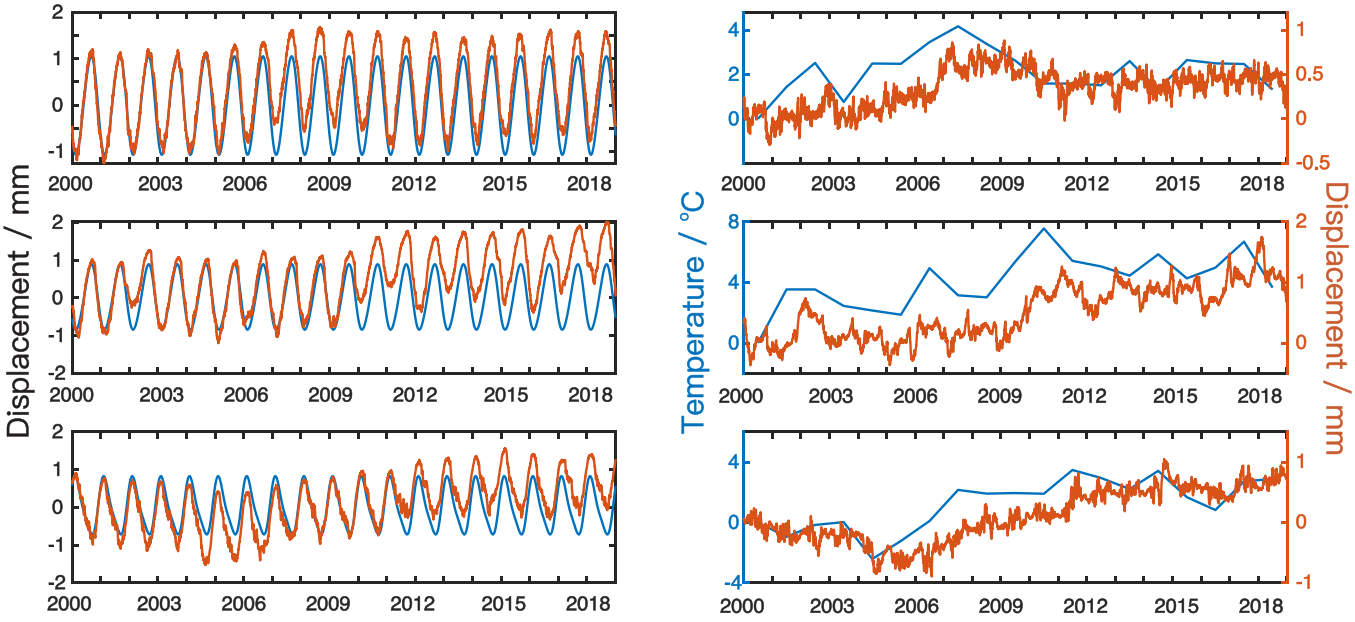

Figure 1. TED time series of GUAO (top), LHAZ (middle) and MCM4 (bottom). The left-hand panels are the TED time series calculated by FEM (red) and the harmonic method (blue). The right-hand panels are the corresponding difference (red, FEM solution minus harmonic solution) and the local mean annual temperature (blue).

derived from the nontidal atmospheric surface pressure obtained from 0.5° × 0.5° 3-hourly the European Centre for Medium-Range Weather Forecasts operational data (Tregoning & van Dam, 2005). Hydrological loads are obtained from the global hydrological model LSDM on a regular 0.5° × 0.5° global grid (Dill & Dobslaw, 2013). Nontidal ocean mass loads are derived from the 3-hourly ocean bottom pressure on a regular 1.0° × 1.0° global grid from the MPIOM ocean model (van Dam et al., 2012). Notably, the environment loads vary among different data centers (Jiang et al., 2013; Zou et al., 2014). Since our main purpose is to study the impact of bedrock thermal expansion on the GPS height time series, only the Deutsche GeoForschungsZentrum (GFZ) products are selected here for reference (Dill & Dobslaw, 2013).

The annual amplitudes and phases of the GPS height time series, mass loads, and mass loads + TED are shown as arrows in Figure S5. Both the FEM and the harmonic method give identical annual amplitudes and phases; therefore, we show only the FEM results as an example. Compared with the mass loads, the annual signal of mass loads + TED is closer to that of GPS. Figure 2 shows the annual amplitude reduction ratio of the GPS height time series after mass loads + TED correction for the total 2,002 sites (the reduction ratio after mass loads correction is shown in Figure S6), with the global distribution of the FEM-derived annual amplitude as its basemap. We observe that regions with obvious annual signals mainly include the eastern and northern parts of Asia as well as the northern part of Canada, with a maximum amplitude of more than 1.8 mm. This finding is consistent with the values obtained by harmonic methods implemented by other investigators (Xu et al., 2017; Yan et al., 2009), which further proves the effectiveness of our FEM method. Regions with weak annual signals are concentrated near the equator, where the temperatures remain high throughout the year. The higher the reduction ratio, the more consistent the annual signals of GPS and models, indicating that the models can better interpret the annual signal in the GPS time series. After mass loads + TED correction, the annual amplitudes are reduced at 1,829 sites (91% of the total sites), with a mean reduction ratio of 55%. If considering only mass loads, the mean reduction ratio is 47% (Figure S6), which indicates that bedrock thermal expansion can explain approximately 8% of the GPS-observed annual signal. Sites with negative ratio reductions (173, 9% of the total sites) are mainly located on islands, at the equator, and in Antarctica, possibly due to the defects of the geophysical models that we used in these regions or uninterpreted geophysical signals that are out of phase with the models, for example, loads of ice sheets.

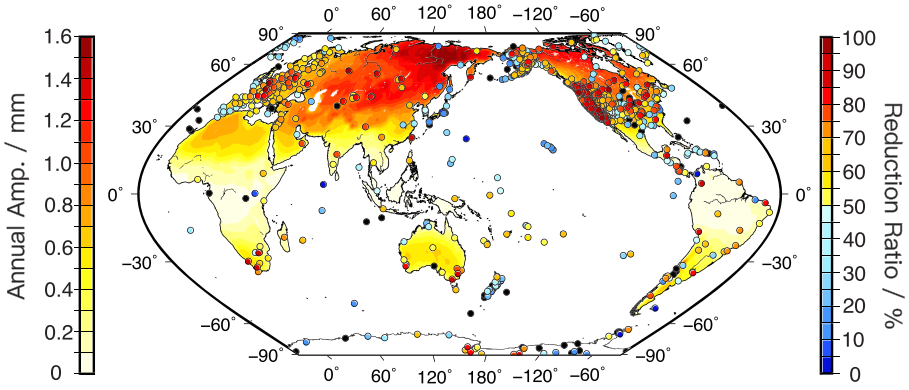

Figure 2. Reduction ratio of annual amplitudes for 2,002 GPS height time series after correction by mass loads + TED. The annual amplitudes of 1,829 (91%) sites are reduced, with an average reduction ratio of 55%. The basemap shows the global distribution of the FEM-derived annual amplitude.

3.3. Nonseasonal Variations of the Bedrock Thermal Expansion Displacement

We subtract the seasonal terms from the full-spectrum TED time series calculated by the FEM to obtain the nonseasonal variations, and then we calculate its range (maximum minus minimum) from 2000 to 2018 (Figure 3). We observe that the regions with large ranges are mainly concentrated on the land around the Bering Strait, the Russian Siberian plain, and the Tibet Plateau. In these regions, the maximum range may exceed 3 mm, which is approximately the maximum peak-to-peak value of the annual amplitude. In addition, the nonseasonal variations contain both irregular long-term trend and interannual changes and thus cannot be modeled using least squares with simple long-term linear trends (Figure S7). The TED calculated by the existing harmonic methods contains only seasonal terms, while the nonseasonal variations of bedrock TED with millimeter-level magnitude are ignored. This ignored signal will remain in the original observations, making the GPS time series more "noisy" and affecting the geophysical interpretation of the geodetic time series. For example, the surface displacement of 1 mm roughly reflects the surface loading mass of a 30-mm equivalent water height. Therefore, the nonseasonal variations of bedrock thermal expansion may partially explain the inconsistency between GPS-inverted and GRACE-observed long-term and interannual changes in the surface mass (Chanard et al., 2014; Han, 2017; Santamaría-Gómez & Mémin, 2015). Furthermore, the regions with large ranges are mainly located on the coast, which means that the bedrock thermal expansion would mostly affect the GPS time series in these regions and thus influence the precise determination of global and regional sea level changes (Mazzotti et al., 2008; Wöppelmann et al., 2007).

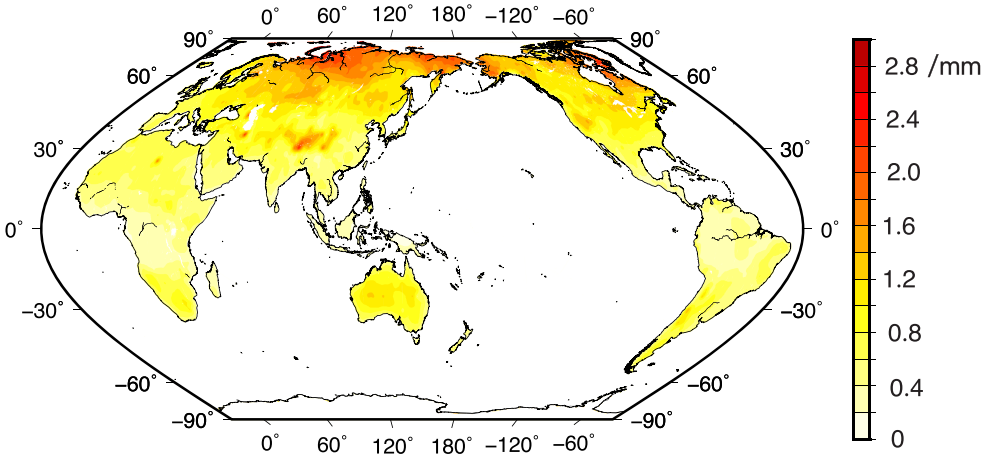

Figure 3. Ranges (maximum minus minimum) of the nonseasonal variations for the TED.

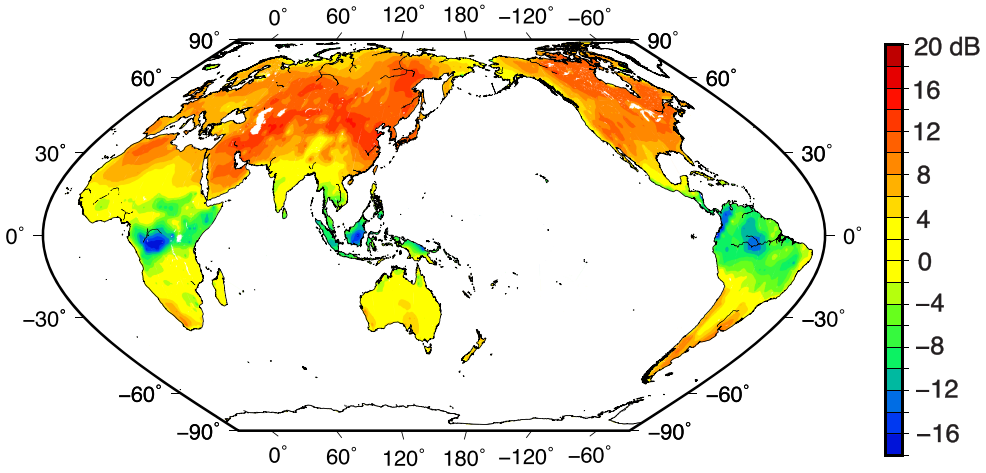

Figure 4. SNR between seasonal terms and nonseasonal variations of the TED.

To investigate whether the GPS daily solutions (Blewitt et al., 1992; Dong et al., 2002; King & Watson, 2010) can detect the TED with millimeter-level magnitude, we calculate the root-mean-square (RMS) of the original GPS height time series, the time series after subtracting the seasonal terms of the TED (harmonic solution), and the time series after subtracting both the seasonal terms plus the nonseasonal variations of the TED (FEM solution) for the selected 2,002 GPS sites. The mean RMS values are 10.48, 10.38, and 10.35 mm, respectively, for these three cases; and station NRIL on the Russian Siberian plain shows the biggest decrease caused by nonseasonal variations, with its RMS values as 12.69, 12.43, and 12.13 mm, respectively. This result indicates that considering the nonseasonal variations would further reduce the GPS scatter by 30% compared with considering only seasonal terms. The RMS decrease also proves that nonseasonal variations do exist and can be detected in the GPS daily solutions, although the magnitude is 1 order smaller than the errors in GPS time series or uncertainties in loading models.

To study the power ratio between the seasonal terms and the nonseasonal variations of the TED, we calculate the "signal-to-noise ratio" (SNR) as follows:

$$SNR = P_s/P_{ns}, \tag{6}$$

where P_s is the power of seasonal terms and P_{ns} is the power of nonseasonal variations. We find that the global SNR distribution shows an obvious regional feature (Figure 4). Seasonal signals dominate most land regions in the middle and high latitudes, while nonseasonal signals are more pronounced around the equator. The mean SNR for all 2,002 GPS sites is approximately 4:1, indicating that, if only the seasonal influence of the TED on the GPS time series is considered, approximately 20% of the full signal would be lost, resulting in an underestimation of bedrock TED.

3.4. The Impact of Physical Parameters and Input Data

Physical parameters and input temperature are crucial to the accurate determination of the TED. With different rock compositions and pressures, the thermal diffusivity κ is in the range of 1–3 mm^2/s (Bording et al., 2016; Clauser & Huenges, 1995; Robertson, 1988), and Poisson's ratio υ is in the range of 0.1–0.4 (Turcotte & Schubert, 2014). Using different combinations of κ and υ, the calculated TED may differ by three folds (Figure S8). We select another surface temperature product from NCEP/NCAR (National Centers for Environmental Prediction/National Center for Atmospheric Research) (Kalnay et al., 1996) to analyze the effects of different input data sets on TED (Figures S9–S10). The global distributions of the derived annual amplitude and range from the two selected data sets generally show good consistency. The main differences are in the Andes and the Tibet Plateau, where the annual amplitude differences can reach 1 mm and the range differences can reach 2 mm (Figure S11). This finding indicates that topography is one of the main reasons for the uncertainty in the temperature products (Zhao et al., 2008). Figure S11c shows that the geopotential height data used by the two reanalysis

products have large differences in the Andes and the Tibet Plateau. Due to the simple relation that the rate of temperature decrease is ~6 °C for each 1-km altitude change, the temperature and its TED thus show large differences in the regions. We then calculate the effect of the TED using surface temperature from NCEP/NCAR on the 2,002 GPS height time series, which shows that the mass loads + TED reduces the GPS annual amplitudes by 53%, while the nonseasonal variations account for approximately 23% of the thermal expansion signal. These results imply that, even with some differences, different data sets can obtain similar TED results, while the choice of physical parameters would cause significant differences in the final TED time series. To accurately calculate the TED, it is necessary to conduct an experimental analysis of the physical parameters for the bedrock.

4. Conclusions

FEM can numerically solve geophysical PDEs without being affected by complex geometry or irregular input data. In this paper, we use FEM to numerically calculate the full-spectrum bedrock TED and then study its seasonal and nonseasonal impacts on the global GPS height time series. The maximum annual amplitude of the TED using the skin temperature from ERA5 reanalysis is 1.8 mm, which is consistent with the values obtained by harmonic methods (Xu et al., 2017; Yan et al., 2009). Most importantly, our solution includes nonseasonal variations that were previously ignored. The range of nonseasonal variations can reach up to 3 mm, which is approximately the maximum peak-to-peak value of the annual amplitude. Approximately 20% of the full thermal expansion signal would be lost if the impacts of the nonseasonal TED variations on the geodetic observations were not considered. This “noise” could be misinterpreted as other signals, which may result in an incorrect geophysical inversion.

Acknowledgments
The work was substantially supported by grants from the National Key Research and Development Program of China (2016YFB0501803, 2017YFA0603104), the Hong Kong RGC Joint Research Scheme (E-PolyU501/16), and the State Key Program of National Natural Science Foundation of China (41531069). The ERA5 reanalysis data set in this analysis is available at https://cds.climate.copernicus.eu, the NCEP/NCAR reanalysis data set is available at https://www.esrl.noaa.gov/psd/data/gridded/data.ncep.reanalysis.html, the GPS time series are available at http://garner.ucsd.edu/pub/timeseries/measures/ats/, and the GFZ environment loads are available at http://rz-vm115.gfz-potsdam.de:8080/repository.

References

Berger, J. (1975). A note on thermoelastic strains and tilts. *Journal of Geophysical Research*, *80*(2), 274–277. https://doi.org/10.1029/JB080i002p00274

Blewitt, G., Heflin, M. B., Webb, F. H., Lindqwister, U. J., & Malla, R. P. (1992). Global coordinates with centimeter accuracy in the International Terrestrial Reference Frame using GPS. *Geophysical Research Letters*, *19*(9), 853–856. https://doi.org/10.1029/92GL00775

Bording, T. S., Nielsen, S. B., & Balling, N. (2016). The transient divided bar method for laboratory measurements of thermal properties. *Geophysical Journal International*, *207*(3), 1446–1455. https://doi.org/10.1093/gji/ggw278

Chanard, K., Avouac, J. P., Ramillien, G., & Genrich, J. (2014). Modeling deformation induced by seasonal variations of continental water in the Himalaya region: Sensitivity to Earth elastic structure. *Journal of Geophysical Research: Solid Earth*, *119*, 5097–5113. https://doi.org/10.1002/2013JB010451

Clauser, C., & Huenges, E. (1995). Thermal conductivity of rocks and minerals. In T. J. Ahrens (Ed.), *Rock physics and phase relation: A handbook of physical constants*. AGU Reference Shelf (Vol. 3, pp. 105–126). Washington, DC: American Geophysical Union.

Dill, R., & Dobslaw, H. (2013). Numerical simulations of global-scale high-resolution hydrological crustal deformations. *Journal of Geophysical Research: Solid Earth*, *118*, 5008–5017. https://doi.org/10.1002/jgrb.50353

Dong, D., Fang, P., Bock, Y., Cheng, M. K., & Miyazaki, S. I. (2002). Anatomy of apparent seasonal variations from GPS-derived site position time series. *Journal of Geophysical Research*, *107*(B4), ETG-9. https://doi.org/10.1029/2001JB000573

Fang, M., Dong, D., & Hager, B. H. (2013). Displacements due to surface temperature variation on a uniform elastic sphere with its centre of mass stationary. *Geophysical Journal International*, *196*(1), 194–203. https://doi.org/10.1093/gji/ggt335

Feng, G., Hetland, E. A., Ding, X., Li, Z., & Zhang, L. (2010). Coseismic fault slip of the 2008 Mw 7.9 Wenchuan earthquake estimated from InSAR and GPS measurements. *Geophysical Research Letters*, *37*. https://doi.org/10.1029/2009GL041213

Fu, Y., Argus, D. F., & Landerer, F. W. (2015). GPS as an independent measurement to estimate terrestrial water storage variations in Washington and Oregon. *Journal of Geophysical Research: Solid Earth*, *120*, 552–566. https://doi.org/10.1002/2014JB011415

Fu, Y., Freymueller, J. T., & Jensen, T. (2012). Seasonal hydrological loading in southern Alaska observed by GPS and GRACE. *Geophysical Research Letters*, *39*. https://doi.org/10.1029/2012GL052453

Galetzka, J., Melgar, D., Genrich, J. F., Geng, J., Owen, S., Lindsey, E. O., et al. (2015). Slip pulse and resonance of the Kathmandu basin during the 2015 Gorkha earthquake, Nepal. *Science*, *349*(6252), 1091–1095. https://doi.org/10.1126/science.aac6383

Han, S. C. (2017). Elastic deformation of the Australian continent induced by seasonal water cycles and the 2010–2011 La Niña determined using GPS and GRACE. *Geophysical Research Letters*, *44*, 2763–2772. https://doi.org/10.1002/2017GL072999

Hao, M., Freymueller, J. T., Wang, Q., Cui, D., & Qin, S. (2016). Vertical crustal movement around the southeastern Tibetan Plateau constrained by GPS and GRACE data. *Earth and Planetary Science Letters*, *437*, 1–8. https://doi.org/10.1016/j.epsl.2015.12.038

Hersbach, H. (2018). Operational global reanalysis: Progress, future directions and synergies with NWP. European Centre for Medium Range Weather Forecasts. https://www.ecmwf.int/en/elibrary/18765-operational-global-reanalysis-progress-future-directions-and-synergies-nwp

Ji, K. H., & Herring, T. A. (2011). Transient signal detection using GPS measurements: Transient inflation at Akutan volcano, Alaska, during early 2008. *Geophysical Research Letters*, *38*. https://doi.org/10.1029/2011GL046904

Jiang, W., Li, Z., van Dam, T., & Ding, W. (2013). Comparative analysis of different environmental loading methods and their impacts on the GPS height time series. *Journal of Geodesy*, *87*(7), 687–703. https://doi.org/10.1007/s00190-013-0642-3

Kalnay, E., Kanamitsu, M., Kistler, R., Collins, W., Deaven, D., Gandin, L., et al. (1996). The NCEP/NCAR 40-year reanalysis project. *Bulletin of the American Meteorological Society*, *77*(3), 437–472. https://doi.org/10.1175/1520-0477(1996)077<0437:TNYRP>2.0.CO;2

King, M. A., & Watson, C. S. (2010). Long GPS coordinate time series: Multipath and geometry effects. *Journal of Geophysical Research*, *115*. https://doi.org/10.1029/2009JB006543

Koulali, A., Ouazar, D., Tahayt, A., King, R. W., Vernant, P., Reilinger, R. E., et al. (2011). New GPS constraints on active deformation along the Africa–Iberia plate boundary. *Earth and Planetary Science Letters*, *308*(1-2), 211–217. https://doi.org/10.1016/j.epsl.2011.05.048

Liu, Y., Xiao, H., Yao, K., Hu, J., & Wei, H. (2018). Rock-soil slope stability analysis by two-phase random media and finite elements. *Geoscience Frontiers*, *9*(6), 1649–1655. https://doi.org/10.1016/j.gsf.2017.10.007

Mazzotti, S., Jones, C., & Thomson, R. E. (2008). Relative and absolute sea level rise in western Canada and northwestern United States from a combined tide gauge-GPS analysis. *Journal of Geophysical Research*, *113*. https://doi.org/10.1029/2008JC004835

Mercer, J. W., Pinder, G. F., & Donaldson, I. G. (1975). A Galerkin-finite element analysis of the hydrothermal system at Wairakei, New Zealand. *Journal of Geophysical Research*, *80*(17), 2608–2621. https://doi.org/10.1029/JB080i017p02608

Pan, Y., Shen, W. B., Shum, C. K., & Chen, R. (2018). Spatially varying surface seasonal oscillations and 3-D crustal deformation of the Tibetan Plateau derived from GPS and GRACE data. *Earth and Planetary Science Letters*, *502*, 12–22. https://doi.org/10.1016/j.epsl.2018.08.037

Quintal, B., Steeb, H., Frehner, M., & Schmalholz, S. M. (2011). Quasi-static finite element modeling of seismic attenuation and dispersion due to wave-induced fluid flow in poroelastic media. *Journal of Geophysical Research*, *116*. https://doi.org/10.1029/2010JB007475

Robertson, E. C. (1988). Thermal properties of rocks. In *USGS Open File Report* (pp. 88–331). US Geological Survey: Reston, Virginia.

Rychlewski, J. (1984). On Hooke's law. *Journal of Applied Mathematics and Mechanics*, *48*(3), 303–314. https://doi.org/10.1016/0021-8928(84)90137-0

Santamaría-Gómez, A., & Mémin, A. (2015). Geodetic secular velocity errors due to interannual surface loading deformation. *Geophysical Journal International*, *202*(2), 763–767. https://doi.org/10.1093/gji/ggv190

Serpelloni, E., Faccenna, C., Spada, G., Dong, D., & Williams, S. D. (2013). Vertical GPS ground motion rates in the Euro-Mediterranean region: New evidence of velocity gradients at different spatial scales along the Nubia-Eurasia plate boundary. *Journal of Geophysical Research: Solid Earth*, *118*, 6003–6024. https://doi.org/10.1002/2013JB010102

Simpson, G. (2017). *Practical finite element modeling in earth science using Matlab*. Wiley-Blackwell.

Trasatti, E., Kyriakopoulos, C., & Chini, M. (2011). Finite element inversion of DInSAR data from the Mw 6.3 L'Aquila earthquake, 2009 (Italy). *Geophysical Research Letters*, *38*. https://doi.org/10.1029/2011GL046714

Tregoning, P., & van Dam, T. (2005). Atmospheric pressure loading corrections applied to GPS data at the observation level. *Geophysical Research Letters*, *32*. https://doi.org/10.1029/2005GL024104

Turcotte, D., & Schubert, G. (2014). *Geodynamics*. Cambridge, UK: Cambridge University Press.

van Dam, T., Collilieux, X., Wuite, J., Altamimi, Z., & Ray, J. (2012). Nontidal ocean loading: Amplitudes and potential effects in GPS height time series. *Journal of Geodesy*, *86*(11), 1043–1057. https://doi.org/10.1007/s00190-012-0564-5

Wöppelmann, G., Miguez, B. M., Bouin, M. N., & Altamimi, Z. (2007). Geocentric sea-level trend estimates from GPS analyses at relevant tide gauges world-wide. *Global and Planetary Change*, *57*(3-4), 396–406. https://doi.org/10.1016/j.gloplacha.2007.02.002

Xu, X., Dong, D., Fang, M., Zhou, Y., Wei, N., & Zhou, F. (2017). Contributions of thermoelastic deformation to seasonal variations in GPS station position. *GPS Solutions*, *21*(3), 1265–1274. https://doi.org/10.1007/s10291-017-0609-6

Yan, H., Chen, W., & Yuan, L. (2016). Crustal vertical deformation response to different spatial scale GRACE and GCMs surface loading. *Geophysical Journal International*, *204*(1), 505–516. https://doi.org/10.1093/gji/ggv385

Yan, H., Chen, W., Zhu, Y., Zhang, W., & Zhong, M. (2009). Contributions of thermal expansion of monuments and nearby bedrock to observed GPS height changes. *Geophysical Research Letters*, *36*. https://doi.org/10.1029/2009GL038152

Zhao, T., Guo, W., & Fu, C. (2008). Calibrating and Evaluating Reanalysis Surface Temperature Error by Topographic Correction. *Journal of Climate*, *21*(6), 1440–1446. https://doi.org/10.1175/2007jcli1463.1

Zou, R., Freymueller, J. T., Ding, K., Yang, S., & Wang, Q. (2014). Evaluating seasonal loading models and their impact on global and regional reference frame alignment. *Journal of Geophysical Research: Solid Earth*, *119*, 1337–1358. https://doi.org/10.1002/2013JB010186